Electrokinetic Instability Micromixing

M. H. Oddy,* J. G. Santiago, and J. C. Mikkelsen

Department of Mechanical Engineering, Stanford University, Building 500, Room 500Y, Stanford, California 94305

We have developed an electrokinetic process to rapidly stir micro- and nanoliter volume solutions for microfluidic bioanalytical applications. We rapidly stir microflow streams by initiating a flow instability, which we have observed in sinusoidally oscillating, electroosmotic channel flows. As the effect occurs within an oscillating electroosmotic flow, we refer to it here as an electrokinetic instability (EKI). The rapid stretching and folding of material lines associated with this instability can be used to stir fluid streams with Reynolds numbers of order unity, based on channel depth and rms electroosmotic velocity. This paper presents a preliminary description of the EKI and the design and fabrication of two micromixing devices capable of rapidly stirring two fluid streams using this flow phenomenon. A high-resolution CCD camera is used to record the stirring and diffusion of fluorescein from an initially unmixed configuration. Integration of fluorescence intensity over measurement volumes (voxels) provides a measure of the degree to which two streams are mixed to within the length scales of the voxels. Ensemble-averaged probability density functions and power spectra of the instantaneous spatial intensity profiles are used to quantify the mixing processes. Two-dimensional spectral bandwidths of the mixing images are initially anisotropic for the unmixed configuration, broaden as the stirring associated with the EKI rapidly stretches and folds material lines (adding high spatial frequencies to the concentration field), and then narrow to a relatively isotropic spectrum at the well-mixed conditions.

Microfluidic devices that perform various chip-based chemical and biological analyses have received significant attention over the past decade. Miniaturization offers key advantages including the following: higher throughput by way of parallelization; shorter analysis times; reduced sample volumes; the possibility for in situ operation; and reduced operation and manufacturing costs.[1]

Miniaturized bioanalytical systems attempt to incorporate many of the necessary components and functionality of a typical laboratory on the surface of a substrate. Typical μTAS components include reaction chambers, pumps, flow sensors, micromixers, diluters, and preconcentrators. Analyses requiring rapid mixing include immunoassays, DNA hybridization, and general cell–molecule interaction. Application of these techniques requires mixing of reagents that often have relatively low diffusion coefficients. Rapid homogeneous mixing becomes increasingly important when the time scale associated with mixing is larger or of the same order as a chemical reaction time scale. In small-scale devices, low Reynolds number (*Re*) flow fields can result in mixing processes on the order of tens of seconds or greater.[2,3] This is particularly true of solution streams containing macromolecules (e.g., globular proteins) whose diffusion coefficients are 1–2 orders of magnitude lower than that of most liquids.

The EKI micromixer, which we present here, is an active micromixer with no moving parts that takes advantage of fluctuating electric fields to effect mixing. We have observed a flow instability in electroosmotic microflows driven with sinusoidally alternating electric fields.[4,5] The EKI has been visualized with both submicrometer tracer particles and fluorescent dye concentration fields. At relatively low frequencies (below ~100 Hz), electric field strengths in excess of 100 V/mm, and channel geometries greater than ~50 μm, a departure from the parallel flow of the stable, reciprocating electrokinetic flow base state occurs. In the case of particle visualizations in long straight channels, particles in the unstable field are observed to have three-dimensional motions. In the scalar visualizations, high-concentration regions of injected dyes are rapidly stretched and folded and dye is dispersed within the flow channel.

Various Micromixing Schemes. Most micromixers can be classified as either active or passive. Passive stirring schemes include simple in-plane, lamination, and chaotic advection stirring. Active mixers have moving parts or externally applied forcing functions such as pressure or electric field. Passive mixers typically use channel geometry to increase the interfacial area between the liquids to be mixed. These mixers can be categorized into two subclasses: in-plane mixers, which divide and mix streams within a fluid network confined to one level (i.e., a pattern that can be projected onto a single plane), and out-of-plane or lamination mixers, which use three-dimensional channel geometries. The simplest in-plane mixers merge two fluid streams into a single channel and accomplish mixing by molecular diffusion. More elaborate in-plane mixers include those of Jacobson et al.[6] and Koch et al.[7] Out-of-plane, lamination mixers can sequentially

(2) Ramsey, J. M.; Jacobson, S. C.; Knapp, M. R. *Nat. Med.* **1995**, *1*, 1093–1096.

(3) Manz, A.; Harrison, D. J.; Verpoorte, E.; Widmer, H. M. *Adv. Chromatogr.* **1993**, *33*, 1–66.

(4) Oddy, M. H.; Mikkelsen, J. C.; Santiago, J. G. Poster presented at the The International Mechanical Engineering Conference and Exposition, ASME, Orlando, FL, 2000.

(5) Oddy, M. H.; Santiago, J. G.; Mikkelsen, J. C. *Proceedings of the Micro Total Analysis Systems Symposium*, Monterey, CA, 2001.

(6) Jacobson, S. C.; McKnight, T. E.; Ramsey, M. J. *Anal. Chem.* **1999**, *71*, 4455–4459.

(7) Koch, M.; Chatelain, D.; Evans, A. G. R.; Brunnschweiler, A. *J. Micromech. Microeng.* **1998**, *8*, 123–126.

* Corresponding author: (fax) (208) 439-0537; (e-mail) oddy@stanford.edu.
(1) Kutter, J. P. *Trends Anal. Chem.* **2000**, *19*, 352–363.

split and stack fluid streams in a three-dimensional fluidic network.[8] Such mixers can achieve exponential growth of stream-to-stream interfacial area for multiple split-and-stack cycles. Microplume array injection is another out-of-plane mixer.[9] A third type of passive mixer is a chaotic advection micromixer;[10] which takes advantage of rapid stretching and folding of material lines associated with pressure-driven chaotic advection.[11] Lamination mixers typically need multilayer microfabrication techniques, which make them less attractive to bioanalysis system designers. This is particularly true for electrokinetic systems where one- or perhaps two-layer fabrication is the norm.

A few active micromixers have been demonstrated. Liepmann and Evans[12] presented a mixing chamber designed to effect fluid stirring using microfabricated valves and phase-change liquid micropumps. Pressure disturbances have also been added to microchannel flows to induce rapid stirring.[13] Although active mixers with moving parts are effective, they are often difficult to fabricate and control and are mostly suited for silicon substrates. An example of a field-driven, active mixer is a mixer being developed by Lee et al.[13] that takes advantage of dielectrophoresis to stir material in a silicon microfabricated mixer.

ALTERNATING CURRENT ELECTROKINETICS: THE STABLE, BASE STATE

We present here a simple treatment of the stable, base state for an oscillating, electroosmotic flow in a two-dimensional microchannel. This analysis identifies interesting nondimensional parameters in the problem and is of interest to researchers who may wish to formulate a stability analysis. We consider the application of a sinusoidally alternating electric field on an electrolyte bounded by dielectric, flat plates of infinite extent. The steadily oscillating velocity profile induced by the harmonic motion of thin electric double layers is presented.

Electroosmotic flow takes advantage of the spontaneous separation of charge generated at a liquid/solid interface, called the electric double layer (EDL). The thickness of the diffuse ion region of the EDL is on the order of the Debye length, λ_D, of the solution and the potential drop across this region is called the zeta potential, ζ. Externally applied electric fields exert a force on the region of net charge, and the ions, in turn, impart a drag force on the bulk fluid.[14] For λ_D, much smaller than a characteristic channel dimension (as in the case of our experiments), the fluid dynamics of the bulk liquid outside of the EDL are well-modeled by a slip velocity boundary condition. This slip velocity is directly proportional to the applied electric field and the local ζ potential. This slip velocity approximation well describes the flow outside of the EDL for applied field frequencies of less than ~1 MHz and

(8) Schwessinger, N.; Frank, T.; Wurmus, H. *J. Micromech. Microeng.* **1996**, *6*, 99–102.
(9) Elwenspoek, M.; Lammerink, T. S. J.; Miyake, R.; Fluitman, J. H. J. *J. MicroMech. Microeng.* **1994**, *4*, 227–245.
(10) Liu, R. H.; Stremler, M. A.; Sharp, K. V.; Olson, M. G.; Santiago, J. G.; Adrian, R. J.; Aref, H.; Beebe, D. J. *J. Microelectromech. Syst.* **2000**, *9*, 190–197.
(11) Aref, H., El Naschie, M. S., Eds. *Chaos Applied to Fluid Mixing*; Pergamon Press: New York, 1995.
(12) Liepmann, D.; Evans, J. D. *Polym. Mater. Sci. Eng. Proc. ACS Div. Polym. Mater. Sci. Eng.* **1997**, *76*, 549.
(13) Lee, Y.-K.; Deval, J.; Tabeling, P.; Ho, C.-H. *Proc. 14th IEEE Workshop MEMS* **2001**, 483–486.
(14) Hunter, R. J. *Zeta Potential in Colloid Science: Principles and Applications*; Academic Press: London, 1981.
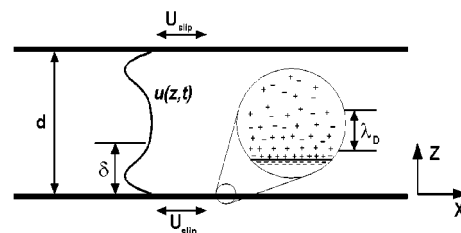
Figure 1. Electrolyte bounded by two infinite flat plates with harmonically oscillating slip condition. The slip condition is applied at the interface between the electrical double layer and the bulk fluid. The three relevant length scales are d, δ, and λ_D. The magnified view shows charges in the double layer, bulk fluid, and wall.

buffer chemistries typical of electrokinetic bioanalytical microsystems.[15]

A schematic of the EDL and flow field is given in Figure 1. The harmonically oscillating flow field may be determined from the Navier–Stokes equations. Assuming a one-dimensional, parallel field, low-Reynolds number flow, the equation of motion for the fluid reduces to

$$\rho \frac{\partial u}{\partial t} = \mu \frac{\partial^2 u}{\partial z^2} \tag{1}$$

With the following boundary conditions,

$$U_{\text{slip}}(y = 0,\, d) = \frac{\epsilon \zeta |E|}{\mu} \exp(i\omega t) \tag{2}$$

Here ϵ is the permittivity of the liquid medium, μ is the dynamic viscosity, and d is the channel depth. Equation 1 is valid in the region outside of the EDL, where the fluid has a net neutral charge. Equation 2, the slip velocity approximation, models the dynamics of the EDL. We obtain an analytic solution to the equation of motion for one-dimensional, steadily oscillating, velocity field by assuming a solution of the form

$$u(z,\, t) = f(z) \exp(i\omega t) \tag{3}$$

The solution to eq 1 with boundary conditions given by eq 2 may be written in nondimensional form as,

$$\hat{u}(\hat{z},\, \hat{t}) = Re\left\{ \frac{\sinh[\beta(1 + i)(1 - \hat{z})] + \sinh[\beta(1 + i)\hat{z}]}{\sinh[\beta(1 + i)]} \exp(i\hat{t}) \right\} \tag{4}$$

where the velocity has been nondimensionalized by the slip velocity. Both time and the transverse spatial coordinate have been nondimensionalized using the forcing frequency and channel depth, respectively. In essence, this is an electrokinetic application of bounded Stokes layers.[16] β is the aspect ratio d/δ and i is the unit imaginary number. The Stokes' penetration depth δ is defined as

(15) Santiago, J. G. *Anal. Chem.* **2001**, *73*, 2353–2365.
(16) White, F. M. *Viscous Fluid Flow*; McGraw-Hill: New York, 1997.
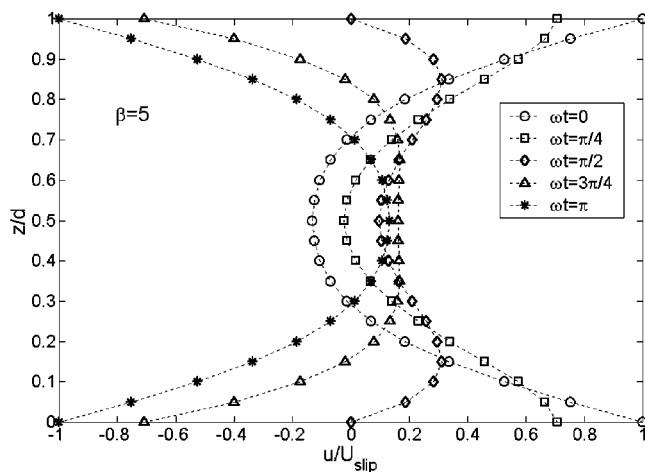
Figure 2. Theoretically predicted velocity profiles for the dynamically stable base state of oscillating flow between two infinite planes. The profiles are plotted for the case where $\beta = 5$ and various nondimensional times in the cycle. Typical values of the Stokes penetration parameter β for which the electrokinetic instability has been observed are approximately in the range of 0.1−10.

$$\delta = \sqrt{2\mu/\rho\omega} \tag{5}$$

Three distinct length scales are revealed in this analysis, namely, d, δ, and λ_D. Given the assumption that the EDL dynamics are coupled to the external flow only through the boundary condition, listing the length scale λ_D serves to ensure that the thin EDL limit is appropriate. The velocity profile of this simple base state flow is shown for various nondimensional times in Figure 2. The velocity profile given by eq 4, reflecting the stable base state has been observed at low field strengths in channels that are well approximated as two-dimensional (i.e., transverse-to-spanwise length ratios of ~8 or greater). The stable base state is not conducive to stirring, but describes the low E-field operation of the mixer and is required for investigations of the hydrodynamic stability of the flow field.

The hydrodynamic stability of the flow profile given by eq 4 is unknown. Hydrodynamic stability analyses have been performed on time-periodic velocity fields that have qualitatively similar features. Von Kerczek and Davis[17] performed a numerical investigation on the hydrodynamic stability of bounded Stokes layers (flow bounded by a harmonically oscillating wall and a stationary wall) for β equal to 8. This large β value simulates the conditions of an unbounded, semi-infinite Stokes layer. Their study showed Stokes layers to be linearly stable to infinitesimal disturbances for Reynolds numbers based on δ and disturbance wavenumbers ranging from $0 < Re_\delta < 800$ and $0.3 < \alpha < 1.3$, respectively. Experimental studies on various oscillatory flows have also been performed. Li[18] used an oscillating flat plate to approximate ideal Stokes layer conditions and reported a critical Reynolds number of 566 for transition to turbulence. Sergeev[19] studied oscillating, pressure-driven pipe flow using a bellows; he reported a transition Reynolds number of 500.

PRELIMINARY EXPERIMENTAL OBSERVATION. ELECTROKINETIC INSTABILITY

We first observed the EKI in a steadily oscillating electro-osmotic flow channel seeded with submicrometer, fluorescent particles. The experimental setup consisted of a simple rectangular borosilicate capillary (Wilmad Labglass, Buena, NJ) of 100 μm × 1 mm inside dimension and a length of 40 mm. The capillary was filled with deionized water and seeded with 490-nm tagged fluorescent polystyrene particles (Interfacial Dynamics Corp., Portland, OR). Particle streaks were imaged using an epifluorescent microscope (Nikon TE300) at 60× magnification (NA = 1.0). A cooled CCD camera (CoolSNAP fx, Roper Scientific, Inc., Trenton, NJ) was used for the image recording. A sinusoidally alternating electric field was applied to the test cell through platinum electrodes introduced into wells (130 μL) at either end of the capillary. The applied voltage was varied from 1 to 8 kV and the frequency was 20 Hz. A surface profile of the channel walls using a profilometer (Alpha-Step, Tencor) indicates that the surface roughness in on the order of 50 nm, or less than 0.1% of the channel depth.

The electric field in this high-aspect ratio, uniform conductivity system is expected to be one-dimensional and to vary sinusoidally in time, yet seed particles were observed to exhibit two- and three-dimensional motions at electric field strengths above 100 V/mm. We observed that the initially uniaxial stable base flow in this system led to apparently random and transverse velocity fluctuations of the seed particles. Sample images of particle streaks in a stable and unstable base flow are shown in Figure 3. The three-dimensionality of the trajectories is apparent since particles are observed to traverse the depth of field of the imaging system. The departure at higher electric field strengths of the one-dimensional particle path lines to three-dimensional path lines, with displacements having components transverse to the applied electric field, suggests that the observed phenomenon is a flow instability. At this time, we do not know if this instability is particular to electrokinetic flows in this regime or if the instability would also be observed in viscous, channel flows with oscillating walls. We are investigating this issue further.

MIXING QUANTIFICATION

We here adopt a terminology similar to that of Eckart,[20] where mixing is divided into two processes: stirring and diffusion. Stirring is a mechanical process, resulting in a redistribution of material such that the net intermaterial area increases. As such, stirring is purely kinematical and dependent only on flow parameters. Diffusion, resulting from random molecular motion, is a material homogenization process on the molecular scale and depends on thermophysical properties such as diffusivity. Stirring enhances mixing, in that it increases the contact area between the streams to be mixed, thereby reducing the necessary diffusion length required for two substances to molecularly diffuse.

Experimental Method. Experimentally, two techniques have been used to study mixing and mixer performance; these are dilution and chemical reaction experiments.[21] Rather than invasively probing the flow directly, the concentration field is typically inferred through fluorescence intensity fields generated from

(17) Von Kerczek, C.; Davis, S. H. *J. Fluid Mech.* **1974**, *62*, 753−773.
(18) Li, H. *Beach Erosion Board.* US Army Corps Engrs *Tech.* Memo 47, 1954.
(19) Sergeev, S. I. *Fluid Dyn.* **1966**, *1*, 121−122.

(20) Eckart, C. *J. Mar. Res.* **1948**, *7*, 265−275.
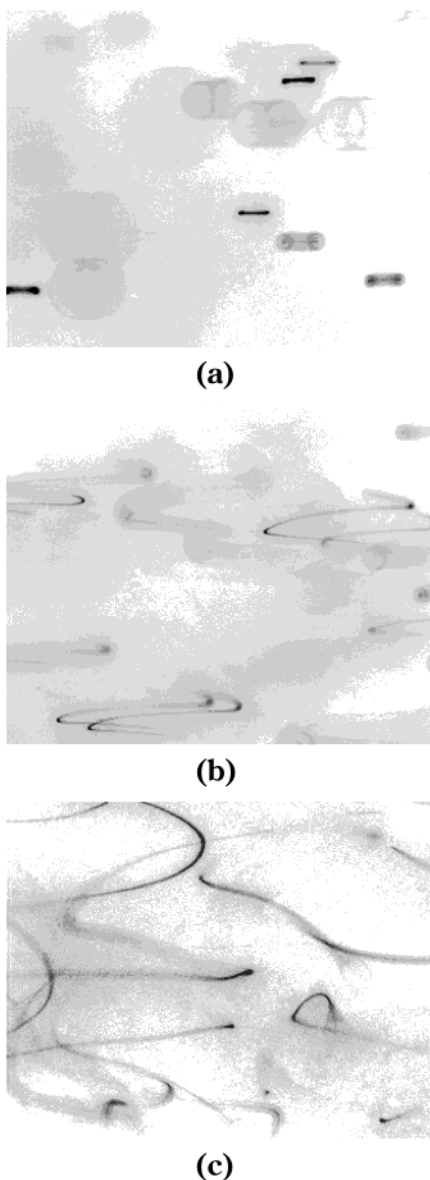(21) Koochesfahani, M. M.; Dimotakis, P. E. *J. Fluid Mech.* **1986**, *170*, 83−112.

Figure 3. Imaged particle path lines for 0.49-μm-diameter tagged fluorescent particles. The image intensity scale here is inverted so that dark streaks represent paths of fluorescent particles. Particle oscillations due to both electrophoresis and electroosmosis are shown for various applied voltages: (a) Uniaxial oscillations in the stable, base state 1 kV. (b) Particles are observed to oscillate with a transverse component at higher applied voltages (4 kV). (c) Particle trajectories in the highly unstable base state (8 kV). In this unstable base state, the flow field is three-dimensional, as particles are observed to traverse the depth of field of the imaging system.

either the dilution or chemical reaction techniques. In a typical dilution experiment, a dyed fluid, consisting of a passive scalar of known concentration, is mixed with an undyed fluid. Note that the data provided by dilution experiments should be carefully interpreted, as the data may overpredict the amount of mixing, due to biasing associated with the finite spatial resolution of the imaging system. A discussion of the biasing that occurs with dilution experiments is given by Karasso and Mungal.[22] Here we applied a dilution technique in order to document the existence of the EKI and to provide a preliminary quantification of the performance of our EKI micromixers.

(22) Karasso, P. S.; Mungal, M. G. *J. Fluid Mech.* **1996**, *323*, 23−63.

Another method of quantifying mixing is through a chemical reaction experiment, which usually uses a fast, irreversible chemical reaction of the type A + B → P, where reactants A and B are mixed to form product P. The yield of product P is a direct measurement of the amount of mixing, since the chemical reaction only proceeds once species A and B have molecularly diffused. Typically, the chemical reaction experiment is performed with an acid−base reaction and a dye having a fluorescence quantum yield that is pH dependent, such as fluorescein.[7,23] We have chosen dilution over this type of reaction-based quantification of mixing in this initial study because of the simplicity of the dilution method and because we wanted to avoid the high pH gradients associated with most reaction experiments. Since electroosmotic mobility (e.g., ζ potential) is a strong function of pH, an EKI micromixer flow field with strong pH gradients is expected to behave significantly different from the homogeneous fluid case presented here.

Imaging Analyses. Two-dimensional, line-of-sight averaged spatial intensity fields are used here to provide a near-instantaneous line-of-sight integration of fluorophores within each imaged voxel. The images were obtained with a spatial resolution of $2.7 \times 2.7~\mu$m in the object plane. A natural metric for quantifying the state of mixedness is the two-dimensional standard deviation of a fluorescence, intensity image obtained from a dilution experiment. As the standard deviation of scalar intensity tends to zero, so would any concentration gradients. However, a well-stirred flow stream can have an arbitrarily high or low standard deviation if molecular diffusion is negligible and the scale of stirring is optically resolved. We therefore use spatial probability density functions (PDFs) of intensities integrated over finite voxel regions to quantify mixing to within the length scales of the voxels. As an example of the reasoning behind this approach, consider two black and white checkerboard spatial intensity distributions having fine and coarse pitches (i.e., two differently "stirred" distributions subject to zero diffusion). These distributions will have identical values for the standard deviation. However, if the intensity distributions are voxel- (or pixel-) averaged over finite regions larger than the smaller of the two pitches (but smaller than the larger pitch), the averaging operation will take into account equal amounts of black and white regions in the fine pitch case, resulting in a unimodal PDF. The voxel-averaged coarse pitch distribution will remain bimodal. PDFs can therefore provide an effective means for interpreting the quality of "mixedness" to within the scale of the voxel.

Power spectra have also been used to quantify the state of mixedness. Power spectra display the spectral content of the image intensity fields. Energy at high spatial frequencies indicates well-resolved dilution experiment images of rapid stirring with little molecular diffusion (or a relatively small amount of unresolved, subpixel stirring). Low-frequency components of image power spectra are associated with both unresolved stirring (i.e., to within the length scales of the line-of-sight integrated images) and well-diffused concentration fields.

MICROMIXER DESIGN AND FABRICATION

We designed and fabricated two micromixing devices that incorporate the EKI as the stirring mechanism for rapidly stirring

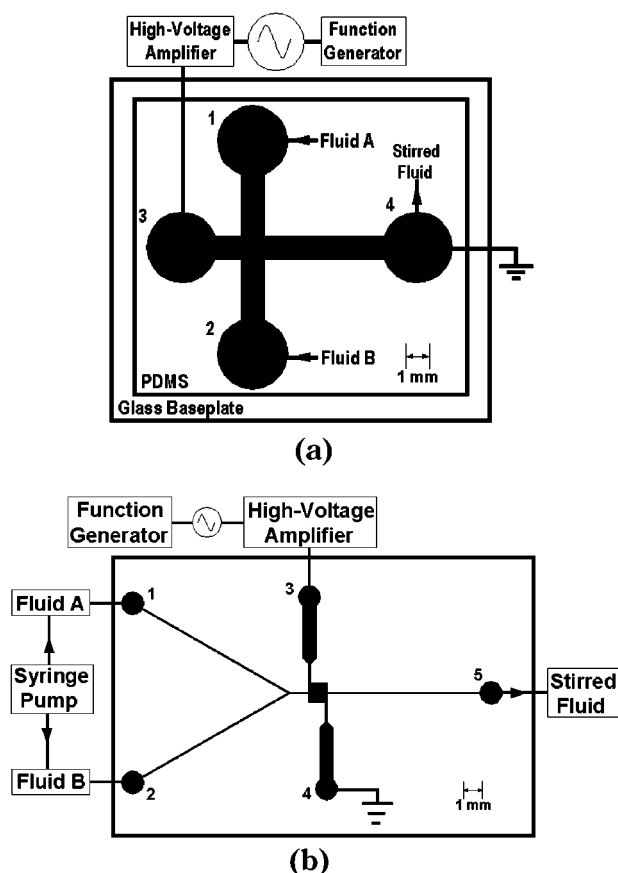(23) Voldman, J.; Gray, M. L.; Schmidt, M. A. *J. Microelectromech. Syst.* **2000**, *9*, 295−302.

Figure 4. Schematics of micromixers I and II: (a) micromixer I channels fabricated from molded PDMS; (b) micromixer II fluidic network microfabricated from wet-etched Borofloat glass substrates. In micromixer II, the electrokinetic instability is confined to the square mixing chamber shown in the center of the schematic and to fluid channel regions within two channel widths (channels are 300 μm wide) from the chamber.

two fluid streams. Micromixer I is a simple, prototype device designed to determine the feasibility of rapidly stirring two fluid streams using the EKI. Micromixer II is a more robust and practical micromixing device capable of stirring a smaller fluid volume either continuously or intermittently.

Micromixer I. A schematic of micromixer I is shown in Figure 4a. The channels have a nominal width and depth of 1 mm and 300 μm, respectively, and were cast in PDMS (Sylgard 184, Midland, MI). The PDMS mixture was first degassed in a vacuum chamber for 1 h and then poured over a mold of the network assembled using rectangular borosilicate glass capillaries (Wilmad Labglass) and epoxy. After curing at 80 °C, the channels were sealed with a glass cover slide. Fluids A and B are introduced into the input ports shown on the left side of the figure. The fluids were pumped through the system using a simple 2 -mm hydrostatic pressure head between inlet and outlet ports. Platinum electrodes introduced into the upstream and downstream reservoirs provided an ac excitation. The EKI occurs along the entire channel.

Micromixer II. A schematic of micromixer II is shown in Figure 4b. The width and depth of the microchannel is 300 μm by 100 μm, respectively. The mixing chamber is 1 mm $\times$ 1 mm $\times$ 100 μm comprising a 0.1-μL volume. The micromixer is an entirely two-dimensional structure fabricated using two Borofloat

glass substrates (Precision Glass & Optics). Standard photolithography and wet-etching processes were used for the microfabrication. A 20-nm chrome layer followed by a 100-nm layer of gold were deposited onto the substrate. A Mylar mask, Shipley S1813 photoresist, and chrome/gold etchants were used to pattern the etch mask. The fluidic network was etched to a depth of 100 μm using pure HF (49%) for ~15 min. In this relatively deep etch process, porosity in the etch mask resulted in some micropitting of the substrate surface, external to the microchannels. The final channel surfaces had roughness elements of about 1−2 μm. After etching, 1-mm-diameter thru holes were drilled through the cover substrate using diamond-tipped drill bits (Triple Ripple Diamond Drill, Lapcraft, Inc., Powell, OH). The fluidic network was sealed by thermally bonding a second borofloat substrate to the etched substrate at 650 °C for 90 min.

For micromixer II, we wanted a mixer design where the instability was largely confined to the mixing chamber and a scheme in which the input flow streams could be driven by either pressure or electric fields. To achieve this, we designed electrical connections with high flow resistance, which mechanically isolate the liquid in the external liquid reservoirs from the liquid in the micromixer chamber. These electrically conductive, high fluidic resistance connections were achieved using porous, dielectric frits (Upchurch Scientific, Oak Harbor, WA) with 0.5-μm pores. Location of the electrodes in buffer reservoirs and isolation of the well from the microchannels using the frits is an effective and robust method for active mixing with an off-chip power source. The design is easily disassembled for frit replacement and is robust to the effects of electrolysis gases produced in the reservoirs.

Two fluids are introduced into the inlet ports 1 and 2 and advected either eletroosmotically or with pressure toward the square mixing chamber. Side channel ports 3 and 4, connected to either side of the mixing chamber, allow for ac excitation. During operation of the mixer, the region of instability and rapid stirring is confined to the mixing chamber and does not penetrate more than two channel widths into the inlet or outlet regions of the main flow channel. Molecular diffusion continues the mixing process while the stirred fluid is advected downstream from the mixing chamber toward port 5.

EXPERIMENTAL PROCEDURE AND IMAGE DATA

For both micromixers I and II, the images provide a line-of-sight integration of the emitted fluorescence along the depth of the microchannels. The intensity registered at each pixel is linearly proportional to the number of fluorophores within the volume element or voxel imaged by each pixel. Images were corrected using flat and dark field images according to the following formula.

$$CI = (OI - DF)/(FF - DF) \qquad (6)$$

where CI, OI, DF, and FF represent the corrected, original, darkfield, and flat-field images, respectively.

Micromixer I. The experimental setup for micromixer I is shown in Figure 5a. A function generator (Hewlett-Packard 33120a) coupled with a high-voltage amplifier (BOP 1000M, Kepco, Inc., Flushing, NY) provided the ac field excitation to platinum electrodes. The frequency and applied voltage were 10
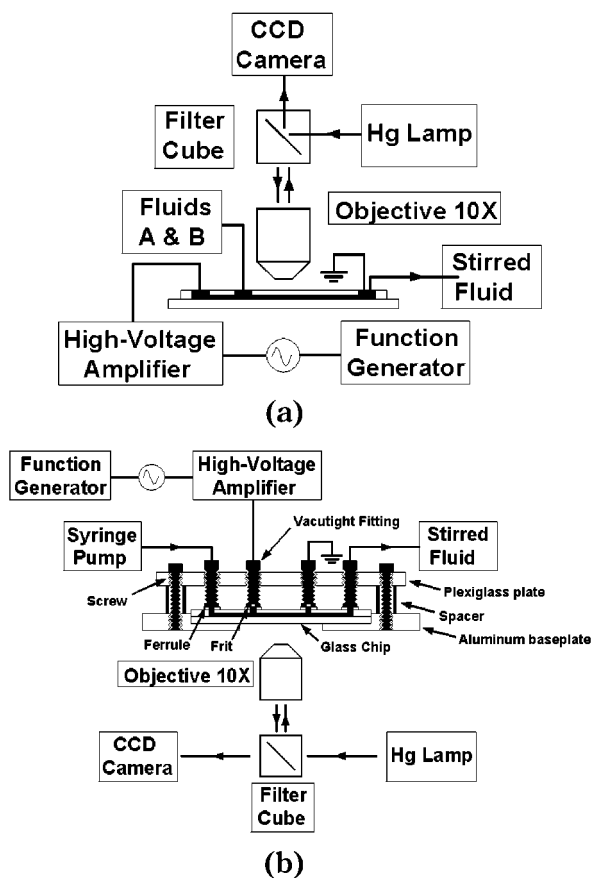
Figure 5. (a) Experimental setup for micromixer I showing optics, fluid paths, and electronics for the mixer. (b) Experimental setup for micromixer II. Micromixer II incorporates external compression fittings attached to mixer excitation side channels. These fittings incorporate porous frits to mechanically isolate liquid in the mixer from the liquid in the reservoirs.

Hz and 1 kV, respectively. The electrode spacing was 9 mm. The working fluid was a 2 mM borate buffer dyed with an order 10 μM solution of 2-MDa dextran/fluorescein conjugate. In all dye visualization experiments discussed here, working fluids were filtered with 0.45-μm pore filters prior to their use.

An upright microscope (Olympus BX40) equipped for epifluorescence was used to view the flow field with a 4× objective (Olympus, NA = 0.1). Illumination from a 100-W mercury lamp was spectrally filtered at the peak fluorescein absorption and emission wavelengths of 485 and 535 nm, respectively, using a filter cube (XF23, Omega Optical, Inc., Brattleboro, VT). Images were captured using a cooled CCD camera (Micromax 1300YHS-DIF, Roper Scientific, Inc.) with a 1300 × 1030 CCD pixel array (square pixels, 6.7 μm on edge) and 12-bit digitization. Image resolution was limited by the point response function (PRF) of the optics, since the diameter of the PRF for the optical setup was 24 μm in the image plane. The camera exposure time was 20 ms.

Time-stamped images obtained from micromixer I are shown in Figure 6. Within 2 s of the application of the ac field, the flow becomes unstable and transverse velocities in the flow quickly stretch and fold material lines. The EKI occurs throughout the 7-mm channel length. The images demonstrate the feasibility of exploiting this flow phenomenon as a stirring mechanism. Pressure-driven bulk flow is from right to left. The application of the

ac field resulted in a rapid deformation of the initial seeded/unseeded fluid interface. The random redistribution of the flow tracer transverse to the applied ac field is evident by the last frame. The instability shown here can be initiated along with a dc electroosmotic flow, with pressure-driven flow (as presented here) or with zero net flow through the channel in "stopped-flow" mode.

Micromixer II. A schematic of the experimental setup for micromixer II is shown in Figure 5b. The ac field was created with a sine wave from a function generator (Hewlett-Packard 33120a) fed into a high-voltage (0 to ±10 kV) amplifier (10/10b, Trek, Inc., Medina, NY). Platinum electrodes were used to apply a voltage and frequency of 4 kV and 5 Hz. Ferrule frits (PEEK, Upchurch Scientific) were added externally to the ac side ports 3 and 4. The measured impedance of the frits in this system is nonnegligible and was measured to be ~2 MΩ for the present experimental conditions.

A syringe pump (PHD2000, Harvard Apparatus, Inc., Holliston, MA) dispensed 0.5 μL/min flow rates into each of the liquid inlet ports. Fluids streams A and B consisted of a 5 mM HEPES buffer, with fluid B dyed with a 20 μM fluorescein solution. The measured electrical conductivities were 160 and 190 μS/cm for the undyed and dyed buffers, respectively. This buffer was chosen in order to minimize the effects of Joule heating in the mixing chamber.

Imaging of dye fluorescence was accomplished using an inverted, epifluorescent microscope (Nikon TE300), a 100-W mercury lamp, and a cooled 12-bit CCD camera (CoolSNAP fx, Roper Scientific, Inc.) with a 1300 × 1030 CCD pixel array of square pixels, 6.7 μm on edge. An XF23 filter cube manufactured by Omega Optical, Inc. was used. Both 4× (Nikon, NA = 0.2) and 10× (Nikon, NA = 0.45) objectives were used, and the exposure time was 2 ms. To increase frame rate, pixels were binned 4 × 4, producing larger pixels with dimensions 26.8 × 26.8 μm in the image plane. The CCD pixel area was larger than the PRF of the optical system; hence, the object-plane voxel dimensions correspond to the pixel area projected onto the object plane.

Figure 7 shows both 4× and 10× objective images of micromixer II in operation. Figure 7a displays a full-field image of the entire mixing chamber including portions of the inlet, exit, and side excitation channels. The images show the rapid stretching and folding of the passive flow tracer. Approximately 2.5 s after the application of the ac field, the mixing chamber fluid is qualitatively well stirred. Figure 7c displays a 1-mm-long portion of the exit channel immediately downstream of the mixing chamber. Once the mixing chamber fluid is well stirred, the output stream of the mixer shows approximately homogeneous fluorescence intensity. The bulk-averaged velocity in the channel and mixing chamber were 0.5 and 0.16 mm/s, respectively. The Reynolds number based on channel depth and rms electroosmotic velocity is 1.5 and the Stokes' penetration depth is 250 μm. Again, the time sequence of images clearly shows the rapid stirring dynamics associated with the EKI. In the section Micromixer Performance Analysis, we present analyses of these images in an effort to quantify the mixing rate.

In addition to the dye visualization experiments presented here, we have visualized 490-nm particles in micromixer II. As in the case of the straight channel flow visualizations described above, the particles were observed to have three-dimensional motions.
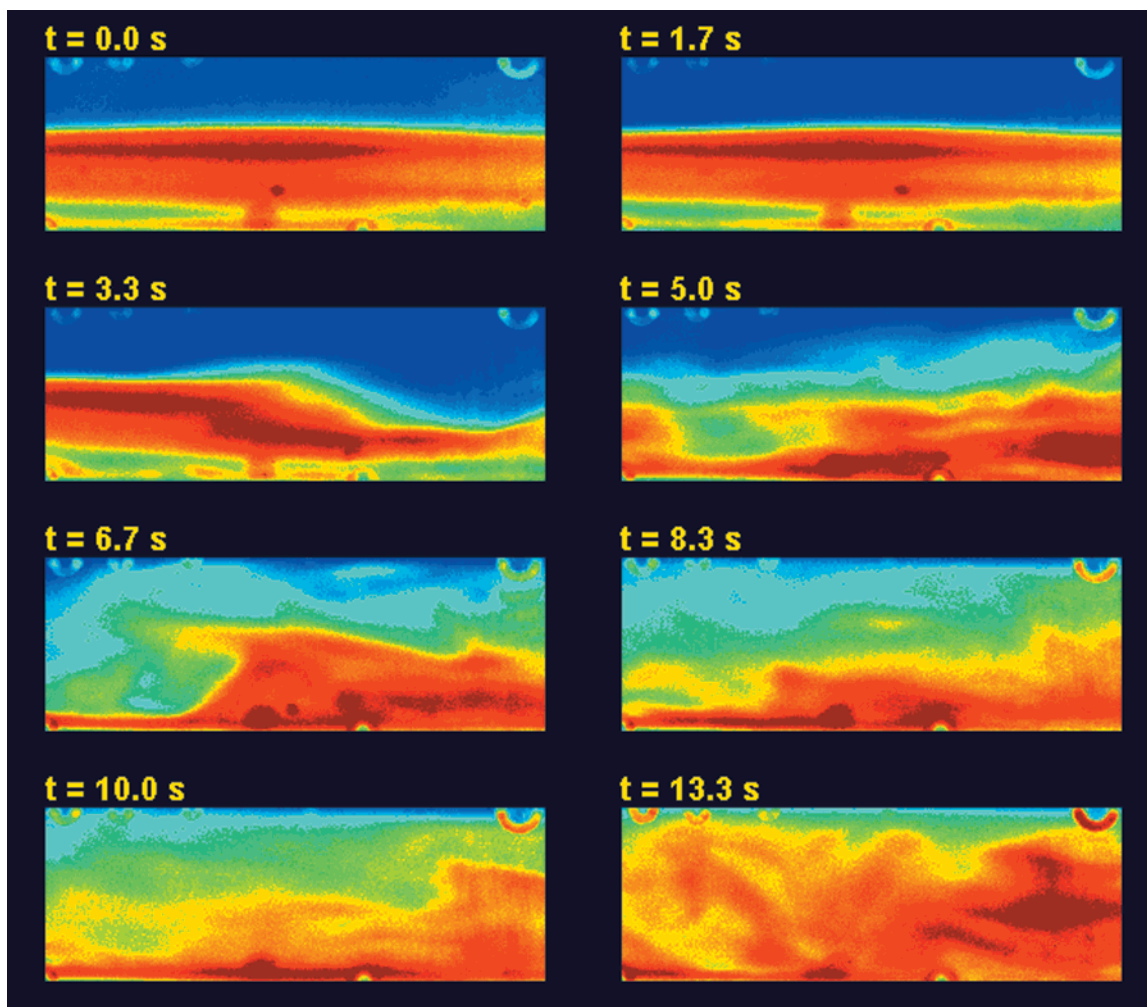
Figure 6. Time-stamped images obtained from micromixer I showing an initially stable interface and its development after the onset of the instability. Some air bubbles are shown clinging to the PDMS channel walls.

Such three-dimensional particle trajectories are not expected in a stable flow field since the electric field is strongly two-dimensional in this uniform depth, fluidic network.

MICROMIXER PERFORMANCE ANALYSIS

We present here performance analyses of micromixer II using both voxel-averaged spatial intensity profiles and direct two-dimensional power spectra of the fluorescence images. The PDF analysis shows the temporal evolution of the voxel-averaged fluorescence intensity probability density as computed from a sequence of near-instantaneous spatial intensity fields. For the PDF calculations, the spatial intensity fields were further binned 4×4, to produce superpixels $100.7 \times 100.7\ \mu m$ in the image plane. The shape of the fluid voxel (i.e., the integrated region of fluorescence imaged by each superpixel) is determined by the optical characteristics of the 25-μm depth of field of the imaging system used. The fluorescence collected by each superpixel is approximately confined to a fluid voxel having an image plane area with an approximate diameter of 30 μm and a depth corresponding to that of the channel. Figure 8 shows results for images within the mixing chamber and for the outflow region immediately downstream of the mixing chamber. Ten instantaneous spatial PDFs of the transient mixing process were ensemble-

averaged over nine realizations. The PDFs are very reproducible from run to run so that each instantaneous PDF is very similar to the ensemble averages shown in the figure. The initially bimodal distribution of voxel-averaged intensities representing the unstirred state quickly tends to a unimodal distribution centered on the steady-state, intermediate intensity of the dilution process. A unimodal intensity distribution is observed 2.5 s after application of the ac field. The standard deviation of these voxel-averaged, intensity PDFs is a measure of the level of mixing for these channels. Figure 9a shows the ensemble-averaged (nine realizations), temporal development of the voxel-averaged PDF standard deviation for the mixing chamber and the channel immediately downstream. The error bars in the plot reflect the 95% confidence intervals across the realizations and are a measure of the high degree of reproducibility of the PDF development.

Image (i.e., nonvoxel-averaged) power spectra for select, representative frames are shown in Figure 10. To reduce frequency leakage, the image data were windowed using an axisymmetric weighted, Bessel function having a peak-to-side lobe ratio of 35 dB:
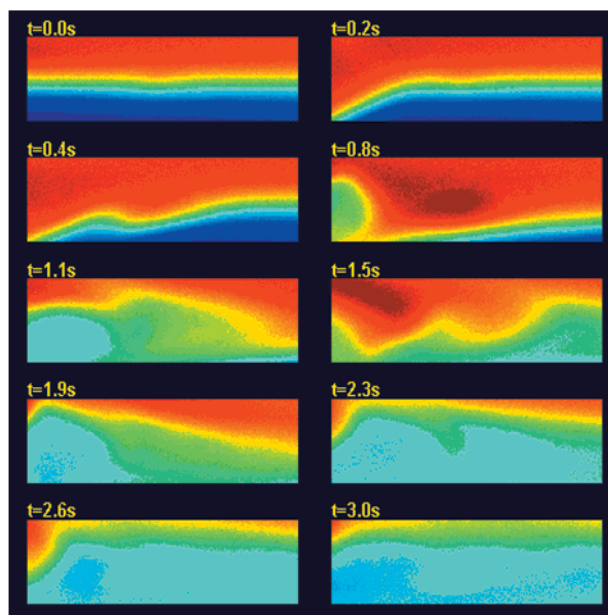
$$w(x,y) = \text{rect}\left(\frac{r}{L}\right)\left[J_0\left(\frac{3.83r}{L}\right) + 0.40\right] \tag{7}$$
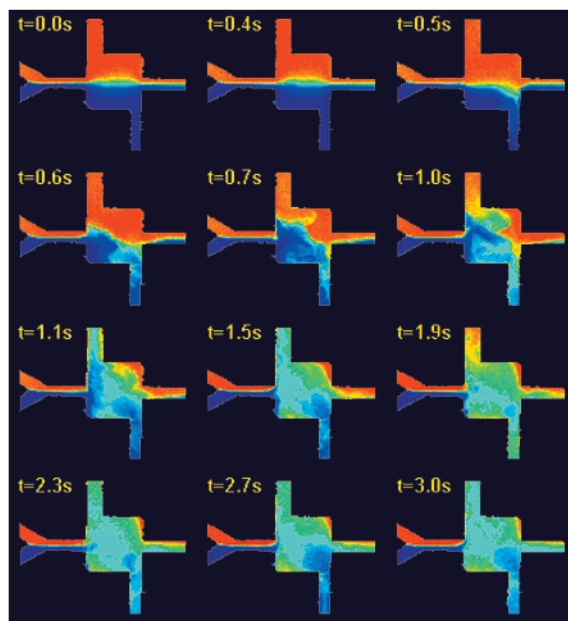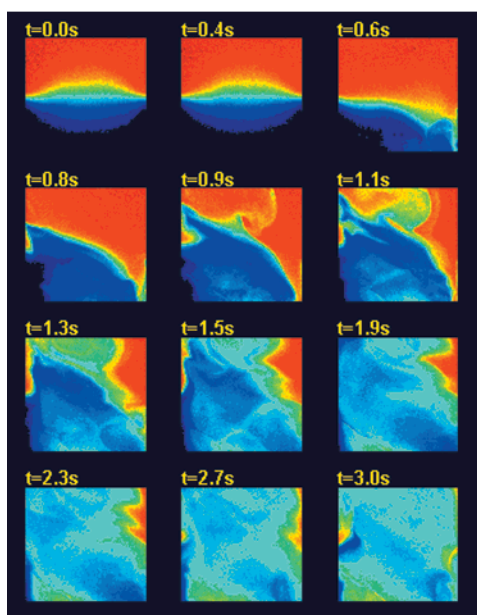
Figure 7. Representative images obtained from micromixer II. (a) 4× objective images displaying the square mixing chamber with inlet, outlet, and side channels. Fluids A and B are continuously advected from left to right. The fluid interface is immediately disturbed upon application of the ac field between the second and third frames. (b) 10× objective images from the square mixing chamber. Complex fluid motions rapidly redistribute dye throughout the majority of the mixing chamber. (c) 10× objective images obtained in the outlet channel, immediately downstream of the mixing chamber. Well-stirred fluid exiting the mixing chamber exhibits a near-uniform intensity profile in the outlet channel.

L is the smaller of either the horizontal or vertical image length. The initially horizontal orientation of the partially diffused dyed/undyed interface results in higher spatial frequencies transverse to the interface as shown by a frequency band that is slightly elongated in the vertical direction. Because the initial interface is partially diffused over a region of ∼230 μm, the harmonics associated with a sharp horizontal interface are not present and the spatial frequency band of the image intensities is confined to 3.1 cycles(cyc)/mm. The transport associated with the stirring motion of the instability has a high ratio of advective to diffusive

flux and the stirring generates high spatial frequency gradients as new, undiffused fluid interface lengths are generated in the flow. This ratio of advective to diffusive fluxes is typically quantified in terms of a Peclet number.[24] Peclet number, UL/D, based on 1-mm chamber dimension and the rms base state velocity, is of order 30 000, where D is the molecular diffusivity of the dye. Parts b−d of Figure 10 clearly show high-frequency components of this high-Pe mixing flow. After sufficient reduction of the mixing

(24) Probstein, R. F. *Physicochemical Hydrodynamics*; John Wiley & Sons: New York, 1994.
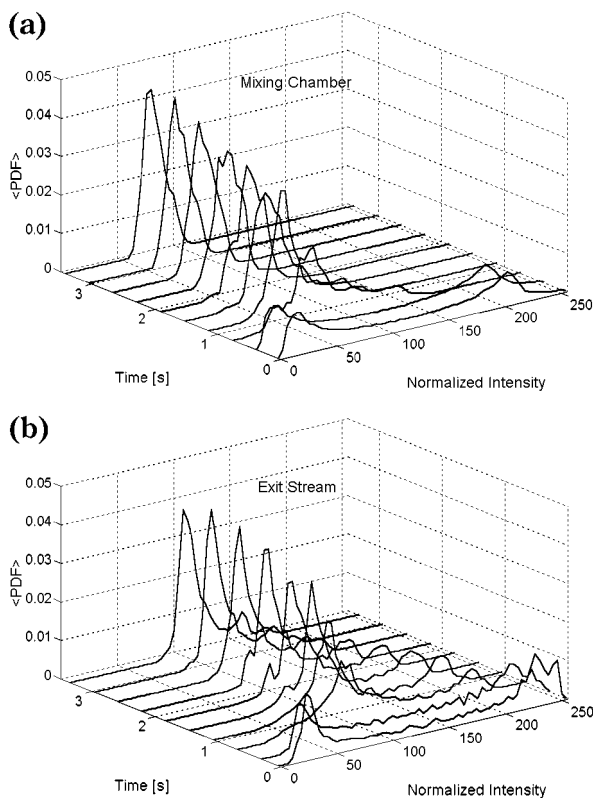
(a)

(b)

Figure 8. Ensemble-averaged temporal evolution of voxel-averaged spatial intensity PDFs. Each ensemble consists of nine realizations. For the PDF analysis, the spatial intensity fields were further binned 4×4, to produce superpixels 100.7×100.7 μm in the image plane. Hence, the dimensions of the fluid voxel correspond to the channel depth of 100 μm and an approximate diameter of 30 μm. (a) The initially distinct dyed and undyed fluids in the mixing chamber exhibit a bimodal distribution that quickly tends to a unimodal distribution upon application of the ac field. (b) Similar behavior is observed in the exit stream immediately downstream of the mixing chamber. The final distribution still exhibits a slight bimodality due to unmixed dye advecting in from a stagnation region near the top right corner of the mixing chamber.

length, diffusion and stirring of the scalar to a scale less than the scales of the imaged voxels quickly damps the high-frequency concentration gradients as indicated by the narrowing of the frequency band to values near the dc peak. This last-stage, high-to-low frequency bandwidth development is particularly evident in the progression from Figure 10c to d. Besides the magnitude of frequency components in the image, the isotropy of power spectra is also a measure of mixing. The intermediate, randomly stirred states of EKI show strongly anisotropic spectra, while the well-stirred state spectra are isotropic.

Figure 11 shows an ensemble-averaged history of the voxel-averaged intensity image bandwidth for the nine-image ensemble discussed above. The bandwidth is here defined as the radius of the frequency band that bounds the spectra that are at least −20 dB of the maximum value. The intensity bandwidth starts at an intermediate value (unmixed case shown in Figure 10a), increases to a maximum as a result of the rapid stirring of the EKI (Figure 10c), and then decreases to a minimum, statistically stationary value for times greater than ~1.5 s. The relatively large magnitude, low-temporal frequency fluctuations in the spatial bandwidth are at the forcing frequency of the applied electric field (5 Hz). These
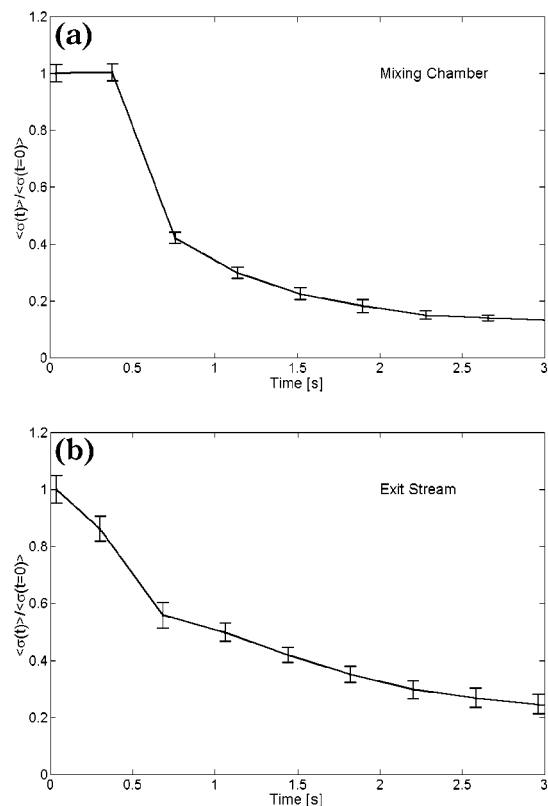

(a)

(b)

Figure 9. Ensemble-averaged standard deviation of PDFs with 95% confidence interval error bars. The initial standard deviation has been used to normalize the curves and the ensemble comprises nine separate realizations. EKI stirring in the mixing chamber (a) and the exit stream (b) show a high degree of reproducibility.

fluctuations are caused by momentary, large-scale displacements of the top and bottom regions of mixer fluid volume into the side ports (and out of the field of view). These fluctuations are quickly damped as the fluids are stirred within the chamber and within the side channel regions near the chamber (see Figure 7a). Again, the error bars reflect 95% confidence intervals across the nine realizations and are a measure of the reproducibility of the bandwidth development in the mixer.

CONCLUSIONS

The ability to rapidly mix fluids at low Reynolds numbers is critical to the functionality of many bioanalytical, microfluidic devices. We have observed an electrokinetic flow instability that occurs at Reynolds numbers as low as order unity and have presented here a demonstration of its application to mixing in microchannels. We have observed the instability in a variety of channel substrates including PDMS, PMMA, and glass. Various electrolytes including deionized water and borate and HEPES buffers, with electrical conductivities ranging from 5 to 250 μS/cm have been used. The microchannel systems presented here clearly show the applicability of the EKI to stirring in on-chip fluidic systems.

Micromixer I is an easily fabricated and operated device that was used to document qualitative features of the instability. Micromixer I demonstrated that the EKI can occur with an electroosmotic flow, a pressure-driven flow, or a flow field with no net flow rate, all with a Reynolds number less than 1.5.
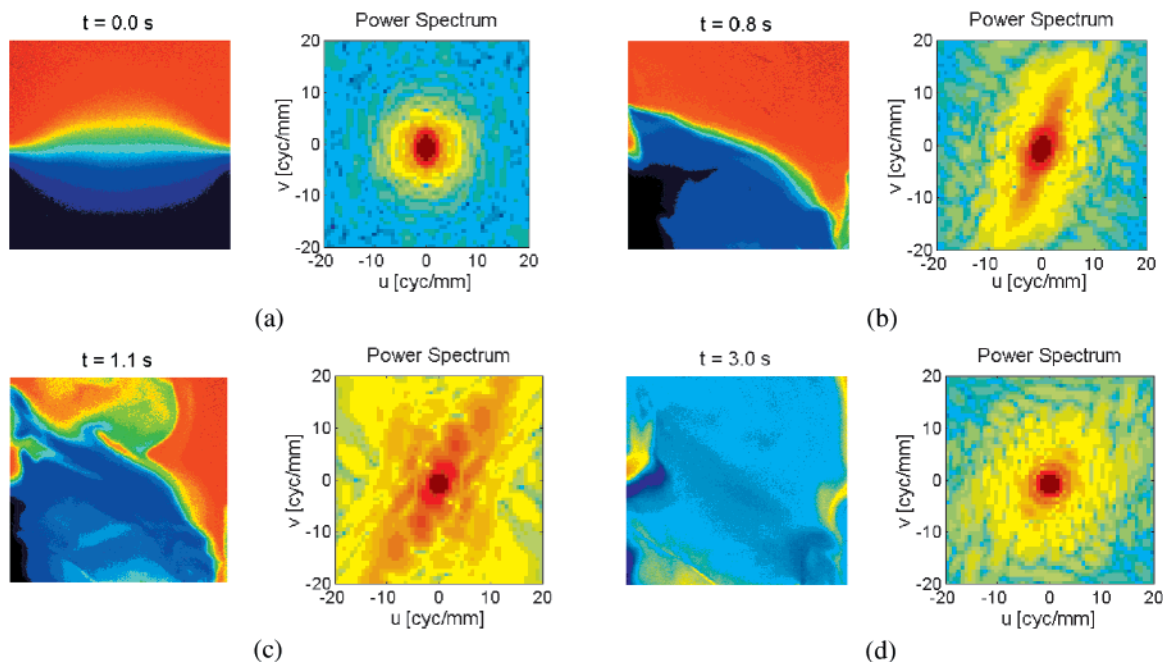
Figure 10. Two-dimensional power spectra of various mixing chamber images. (a) The initial distribution of dye exhibits larger frequency components along the vertical direction. (b, c) Larger spatial frequencies are introduced by the EKI stirring within the chamber. (d) The nearly homogeneous intensity profile of the last frame is indicated by an attenuation of large spatial frequencies.

Micromixer II implemented this stirring mechanism in a more robust device requiring no moving parts. This micromixer design can be incorporated into a single-layer microfabricated fluidic system with only minor modifications to a lithographic mask and the addition of external connections for electrodes. Rapid electrokinetic stirring has been achieved in a "stopped-flow" or continuous-flow mode where the throughput of sample streams is actuated by either pressure or electroosmotic forces. These advantages should allow the device to be easily integrated into current single-layer microfluidic chips with little or no additional fabrication requirements other than simple mask layout changes. Design of mixer geometry with electrode wells within 1 mm of the mixing chamber can probably be used to reduce the required voltages to less than 1 kV. The time scale required for the fluids to become mixed to within the scale of the voxels is reduced by ~2 orders of magnitude for the mixtures studied here.

Both PDFs and power spectra of spatial intensity profiles were used to assess the micromixer performance using a dilution experiment. The time for the voxel-averaged PDF's to reach a unimodal shape provided a measurement of the time for the EKI to stir the fluids to within the length scales of the voxel. For micromixer II, our definition of time to mix was 3 s for two 0.5 μL/min flows in a mixing chamber of dimensions $1 \times 1 \times 0.1$ mm. This time to mix can be compared to the characteristic diffusion time of fluorescein across half the mixer width (0.5 mm), which is 500 s. Note that the simple diffusion-to-stirring time scale ratio for EKI mixing of higher molecular weight molecules should be even greater.

Power spectra provide information regarding the spatial frequency content of the spatial intensity profiles. Initially, the diffused fluid-to-fluid interface resulted in a relatively low bandwidth of 3.1 cyc/mm. Upon the application of the mixing, high-Peclet number stirring increased the frequency band of the intensity fields to a value as high as 4.5 cyc/mm. After 1.2 s, the
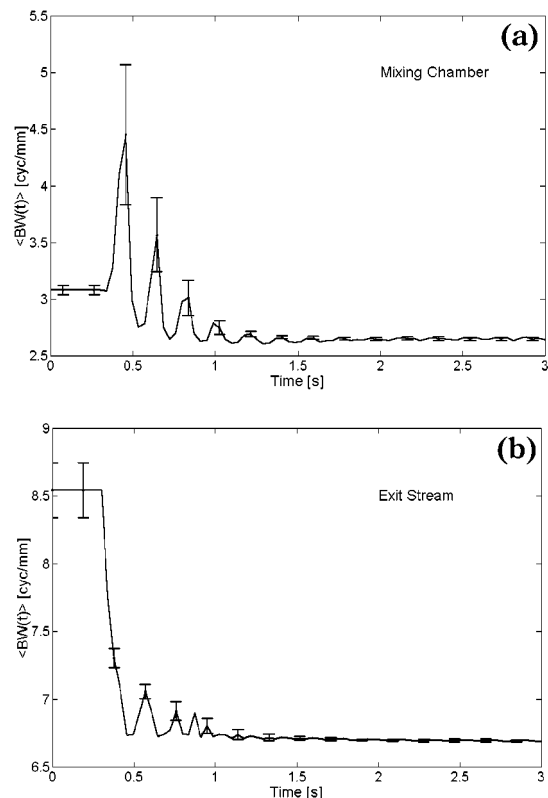

Figure 11. Ensemble-averaged −20 dB bandwidth power spectra shown for both the mixing chamber (a) and the exit stream (b). Error bars are shown with 95% confidence intervals, EKI stirring is observed immediately after the application of the ac field at $t = 0.4$ s. The initial oscillation in the bandwidth is due to large-scale fluid displacements in to and out of the ac excitation side channels. After 1 s of actuation of the EKI, the fluid is sufficiently stirred and the bandwidth remains constant.

three-dimensional motions of the EKI stirred the fluid streams to within the scales of the voxel and reduced the frequency bandwidth to less than 2.7 cyc/mm. The development of the PDFs and the spectra both predicted similar values of time to mix. The PDF evaluation method is easier to compute.

A flow phenomenon that might be compared to the EKI is electrohydrodynamic (EHD) instability.[25,26] The EHD instability is typically observed in fluids classified as leaky dielectrics that have electrical conductivities at least 2−3 orders of magnitude lower than the fluids used here. Unlike strong electrolyte solutions, these dielectric fluids can support space charge in the absence of gradients of properties such as ionic conductivity and permittivity. The dynamics of these net charge fluid regions contribute to the instability development in EHD. Further, Rayleigh−Benard (or a buoyancy-driven) instability is an unlikely cause of the phenomenon we observe. In our geometries, the required temperature differential for achieving the critical Rayleigh number in our flow is more than 4 orders of magnitude higher than the boiling point of our fluid for these 100-μm-deep (the

dimension along the gravitational vector) microchannels. However, temperature gradients should not be entirely discounted as a source of instability. We estimate temperature differences as a result of Joule heating on the order of 5−10 °C for the 3-s duration high-voltage pulse used to stir the fluid in micromixer II. This estimate is based on thermocouple measurements and simple lumped-capacitance heat-transfer analyses. Such temperature differences across the transverse lengths of our flow channels may induce asymmetries in transport coefficients that may ultimately lead to instability. Viscosity is particularly temperature sensitive and can affect asymmetric viscous stresses in the flow.

(25) Schneider, J. M.; Watson, P. K. *Phys. Fluids* **1970**, *13*, 1948−1954.
(26) Melcher, J. R.; Taylor, G. I. *Annu. Rev. Fluid Mech.* **1969**, *1*, 111−146.